SURFACE CHEMISTRY

Ultrasonic tweezer for multifunctional droplet manipulation

Zichao Yuan, Chenguang Lu, Cong Liu, Xiangge Bai, Lei Zhao, Shile Feng, Yahua Liu*

Spatiotemporally controllable droplet manipulation is essential in diverse applications, ranging from thermal management to microfluidics and water harvesting. Despite considerable advances, droplet manipulation without surface or droplet pretreatment is still challenging in terms of response and functional adaptability. Here, a droplet ultrasonic tweezer (DUT) based on phased array is proposed for versatile droplet manipulation. The DUT can generate a twin trap ultrasonic field at the focal point for trapping and maneuvering the droplet by changing the position of the focal point, which enables a highly flexible and precise programmable control. By leveraging the acoustic radiation force resulting from the twin trap, the droplet can pass through a confined slit 2.5 times smaller than its own size, cross a slope with an inclination up to 80°, and even reciprocate in the vertical direction. These findings provide a satisfactory paradigm for robust contactless droplet manipulation in various practical settings including droplet ballistic ejection, droplet dispensing, and surface cleaning.

INTRODUCTION

Controllable droplet manipulation is valuable in various practical applications, such as biological detection (*1*, *2*), chemical reactions (*3*, *4*), water harvesting (*5*–*7*), and heat management (*8*–*10*). Various external stimuli including magnetism (*11*–*15*), electricity (*16*–*19*), and light (*20*–*22*) are introduced to achieve more flexible and precise droplet manipulation on superhydrophobic surfaces. For magnetic actuation, the droplet either chases the trajectory of the underneath permanent magnet via forming a continuous indentation on magnetic responsive surfaces (*11*–*13*) or follows the magnetic beads embedded in the droplet (*14*, *15*). Electric-based manipulation mainly uses the Coulomb force to drive the droplet rapidly via electrostatic repulsion (*16*–*18*) or attraction (*19*). Similarly, leveraging the dielectrophoretic force within the droplet resulting from the photopyroelectric effect, light-based manipulation enables a rich fluidic operation and droplet patterning (*20*–*22*). Despite remarkable progress, it is still a challenge to achieve the contactless droplet manipulation without the need for essential surface or droplet pretreatment, such as preparing a surface with specific properties (*11*, *17*, *21*) and premodifying the electrostatic properties of the droplet (*16*, *19*). Moreover, the driving force to propel the droplets is usually small, which further restricts their versatile applications.

Alternatively, the acoustic levitation leveraging the acoustic radiation force generated in the acoustic field, enabling the particles or liquid droplets to be suspended in air, might open up a promising avenue for droplet manipulation (*23*–*27*). In an effort to circumvent the constraint that the acoustic radiation force is mainly used to counteract the gravity force of the object in the acoustic levitation (*28*, *29*), Marzo *et al.* (*30*) proposed to realize acoustic trapping, translating, and rotating particles based on ultrasonic phased array, i.e., a group of sensors located at distinct spatial locations to enhance the propagation in a desired direction by controlling the relative phases of the sensor signals. An unprecedented acoustic structure, i.e., twin trap, has been generated at the focal point to tweeze the particles in a flexible manner (*31*), which may present an excellent alternative for droplet manipulation benefiting from its robust contactless trapping and flexible control.

In this research, a droplet ultrasonic tweezer (DUT) based on phased array is developed to achieve multifunctional droplet manipulation on superhydrophobic surfaces. The DUT could generate a twin trap ultrasonic field at the focal point to trap and control the water droplet by changing the position of the focal point. We demonstrate that the droplet can move precisely along arbitrarily programmed paths in a fast and efficient manner with a wide volume range. The DUT enables the droplet to pass through a narrow slit much smaller than its own size, cross steep slopes, and even reciprocate in the vertical direction, which yields a superior platform for ballistic droplet ejection, droplet dispensing, chemical reacting, and surface cleaning.

RESULTS

Droplet ultrasonic tweezer

Figure 1A shows the schematic of the DUT, comprising an ultrasonic phased array, and a water droplet on a superhydrophobic surface. The phased array is positioned in a double-layered symmetrical circular pattern with a diameter of 51 mm, e.g., six times that of the ultrasonic wavelength to concentrate the ultrasound energy. Twenty-eight ultrasound transducers in the phased array facing toward the center of the array could emit a sinusoidal ultrasonic signal at 40 kHz, with the ultrasonic intensity being controlled by tuning the relative emission amplitude A (0 to 1) in the control system, which was proposed in a previous work (*32*). Hence, a twin trap ultrasonic field could be created at the focal point, whose position could be managed by the control software. Figure 1 (B and C) visualizes from the numerical simulation the shape of twin trap with two symmetrical tweezer tip–shaped regions and the relative acoustic pressure amplitude distribution of the twin trap, respectively. As indicated by the color gradient from dark to bright in Fig. 1C, the amplitude near the focal point is close to zero in the y and z directions, while it increases and then decreases as far away from the focal point in the x direction with the

State Key Laboratory of High-Performance Precision Manufacturing, Dalian University of Technology, Dalian 116024, P. R. China.
*Corresponding author. Email: yahualiu@dlut.edu.cn

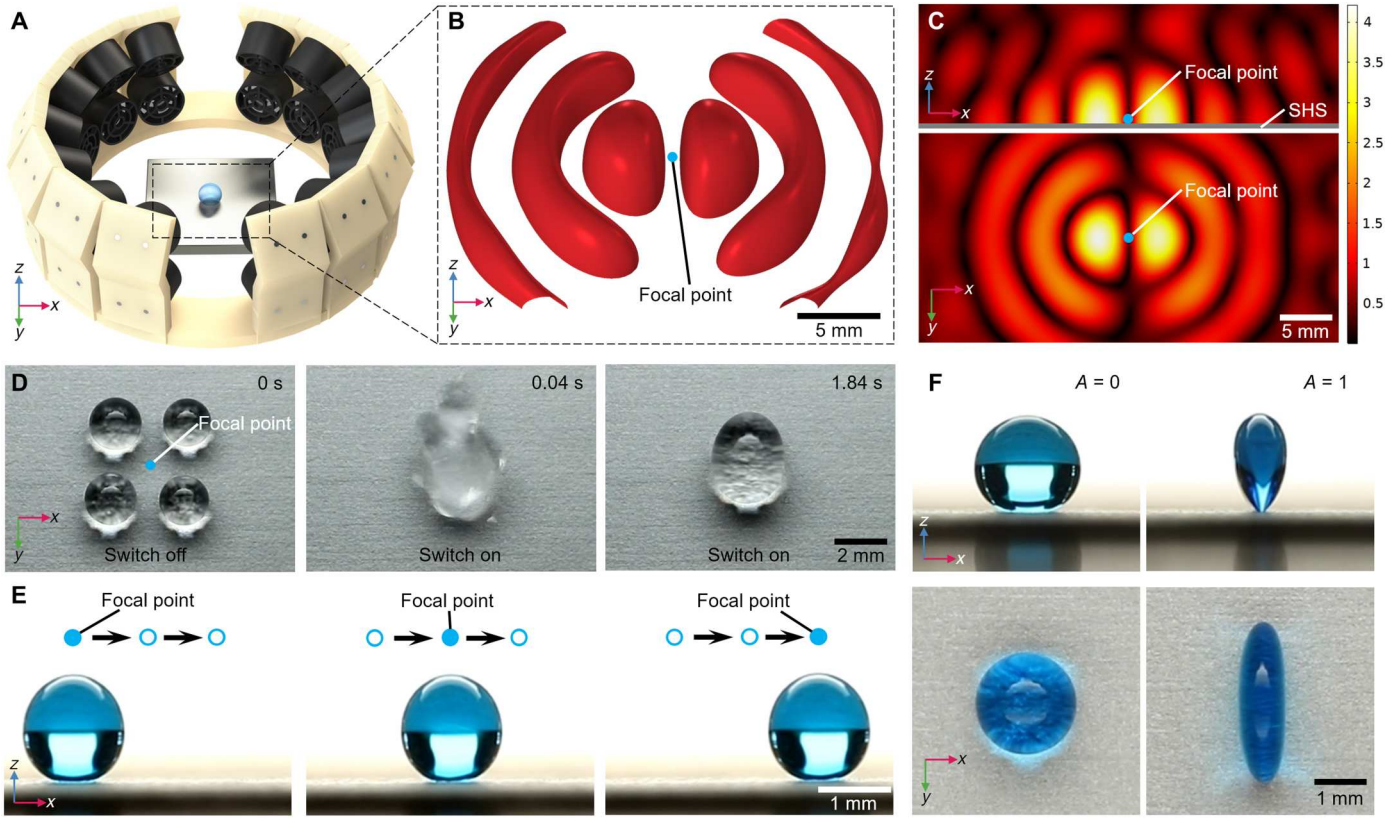

Fig. 1. Ultrasonic field and droplet controllability. (**A**) Schematic of the droplet ultrasonic tweezer (DUT) including ultrasound transducers, a bracket array, and a water droplet on the superhydrophobic surface. (**B**) Simulated shape of twin trap ultrasonic field generated by the DUT. (**C**) Relative acoustic pressure amplitude distribution of the twin trap from the numerical simulation. SHS, superhydrophobic surface. (**D**) Droplet trapping process in the twin trap with $A = 0.4$. (**E**) Sequential images showing the controllability of the DUT by changing the position of the focal point for a 4-μl droplet at $A = 0.4$. (**F**) Deformability of a 4-μl droplet in the twin trap with $A = 1$.

maximum value located in the brightest zone. The consistency of the actual field with the simulation verified the reliability of the simulations, as shown in fig. S1.

To clarify the feasibility of the DUT for droplet manipulation, we investigate the effect of the twin trap on the droplet motion. As shown in Fig. 1D and movie S1, four droplets of ~4 μl are placed on the superhydrophobic surface around the focal point when the DUT is switched off. They converge and merge rapidly and lastly cease at the focal point when the DUT is activated, demonstrating that droplets could be preferably trapped at the focal point in the twin trap. This discovery substantially elevates the droplet controllability of the DUT, i.e., to accurately maneuver a drop by altering the position of the focal point in the x and y directions step by step. As shown in Fig. 1E, a trapped 4-μl droplet follows the focal point and moves from left to right in the x direction for two steps with each step at 1 mm, exactly the same as the moving distance of the focal point in the control software. Note that the position of the focal point in Fig. 1E only represents the position in the horizontal direction, and the actual focal point is on the surface to obtain the maximum ultrasonic intensity. The shape of the droplet is affected by the relative emission amplitude A. Figure 1F shows the side and top views of a 4-μl droplet (left column) placed on a superhydrophobic surface, and it is compressed in the x direction and elongated in the y direction at $A = 1$ (right column).

Multifunctional droplet manipulation

To further demonstrate the dexterous manipulation capabilities of DUT, we move the droplets in diverse terrain situations, such as being guided following an arbitrary programmed trajectory, passing through narrow slits, crossing steep slopes, and migrating against gravity. As shown in Fig. 2A, a 4-μl droplet is trapped and moves precisely along the path "DUT" and along the trajectory of a triangle, square, and circle accurately (fig. S2A and movie S2). These results indicate that the DUT is able to move droplets in any programmed path. Moreover, because of the instant change of the twin trap resulting from the immediate shift of the focal point, the droplet could be maneuvered in real time and move fast in a damping oscillation manner with an average velocity of ~160 mm/s (fig. S2B). A 1-μl droplet can even achieve a maximum velocity of ~254 mm/s (fig. S2C). It is obvious that the droplet manipulation mainly relies on the relative emission amplitude and the droplet volume, and fig. S2D shows a phase diagram describing the maneuverability of droplets with different sizes under various relative emission amplitude A. Notably, a droplet with a suitable size can be well controlled under a proper A (blue region), while mismatched size and A result in an unstable state of the droplet due to its deformable nature of the liquid, either splitting into smaller ones under a large A (fig. S2E and movie S3) or moving randomly (fig. S2F and movie S3). Furthermore, fig. S2G shows the moving process of a 2-μl droplet, with the dashed lines marking

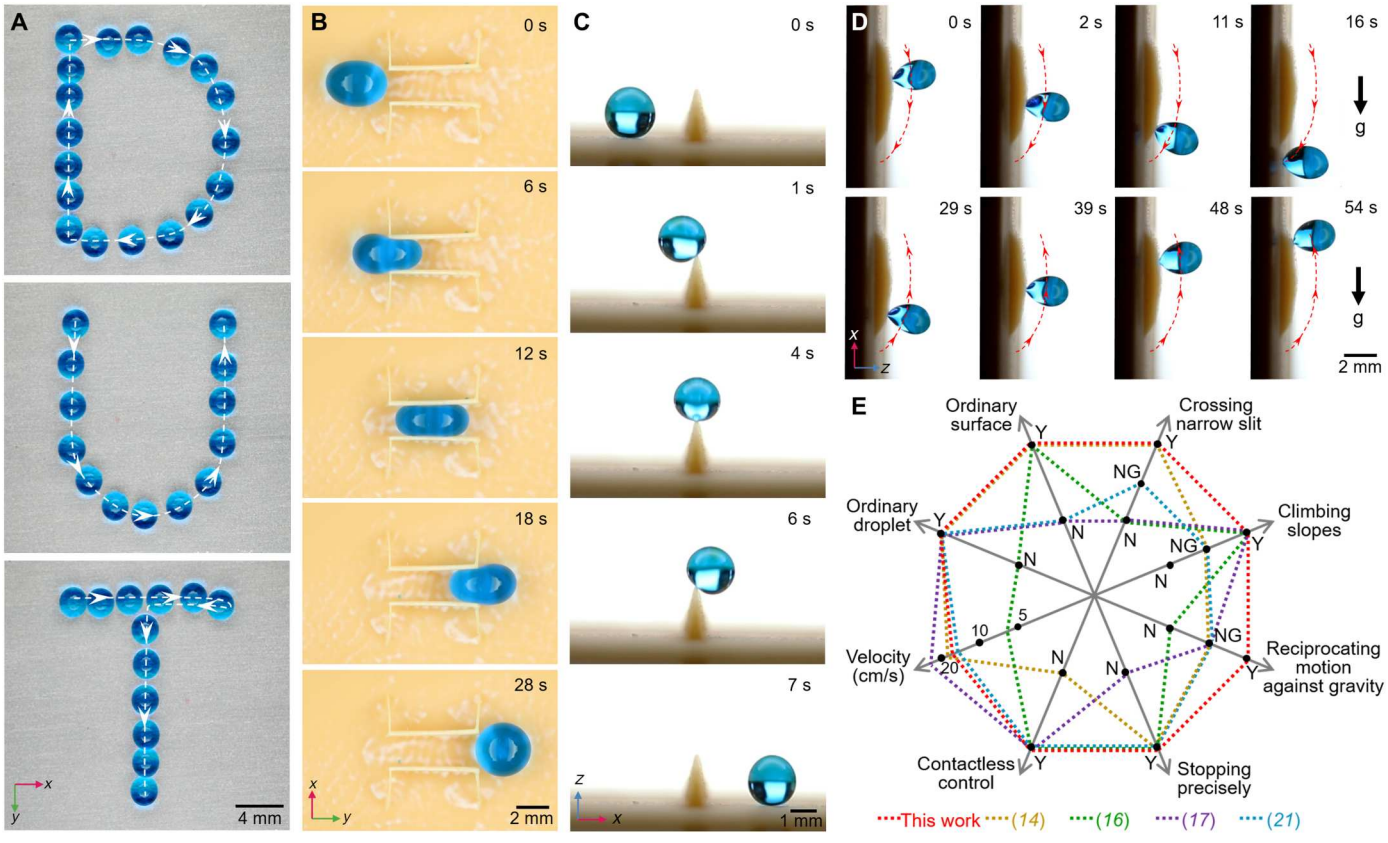

Fig. 2. Multifunctional manipulation of the droplet ultrasonic tweezer (DUT). (**A**) Stacked images of a 4-μl droplet drawing the trajectory of the letter D, U, and T at $A = 0.2$. (**B**) Capability of a 20-μl droplet crossing narrow slit with a width of 2 mm at $A = 0.4$. (**C**) Capability of a 3-μl droplet surmounting steep slope with an inclination up to 80° at $A = 0.4$. (**D**) Capability of a 4-μl droplet moving against gravity in a reciprocating motion on a vertically placed convex surface at $A = 0.4$. (**E**) The notable advantages of the DUT compared with other techniques from eight aspects. The ordinary droplet and ordinary surface refer to the droplet and surface without the need for pretreatment, respectively. The average velocity of the droplet can reach ~160 mm/s (fig. S2B). Y, yes; N, no; NG, not given.

the variation of the advancing and receding contact points. The alternating motion of the advancing and receding contact point indicates a rolling movement of the droplet over the surface during the manipulation process (movie S4).

The well-controlled droplet manipulation is also demonstrated by the capability to traverse a narrow slit with the help of DUT, which has never been reported before. Figure 2B shows a 20-μl droplet moving faithfully through a superhydrophobic narrow slit with a width of 2 mm, and the slit side walls were constructed with mesh to enable a stable control even when the droplet completely squeezes into the slit. Specifically, a droplet of diameter $d = 3.4$ mm is elongated slightly in the y direction when trapped by the DUT. Then, it squeezes into and passes through the slit smoothly as the focal point moves forward (movie S5). Figure S3A further shows the trafficability of droplets with different sizes, where the minimum slit width could be 2.5 times smaller than the droplet's diameter. Except for straight slits, a droplet can also be maneuvered across complicated terrain, e.g., a 6-μl droplet travels through a composite topography of two slopes and an S-shaped slit (fig. S3B and movie S6), which holds potential in the design of soft robotics.

In addition to manipulation on the horizontal dimension, droplet maneuvering including surmounting steep slopes and even reciprocating against gravity on the vertical dimension can be achieved by leveraging DUT, which is usually challenging for other techniques. As shown in Fig. 2C and movie S7, a 3-μl droplet climbs up a slope with an inclination up to 80° and then descends as the focal point keeps moving forward. Specifically, as shown in fig. S4A and movie S8, the droplet first rolls toward the foot of the slope and then leaves the ground and wheels along the slope to the top, indicating that the droplet retains an intimate contact with the surface during the climbing process. Figure S4B further shows the slope-crossing ability of droplets with different sizes for different slope inclinations, e.g., droplets less than 8 μl can go over the slope with an inclination 80°. Moreover, the DUT endows the droplet to climb the slope whose height is larger than its own size, e.g., a 4-μl droplet crosses a 40° slope with the maximum height of 2.5 mm (fig. S4C and movie S9), which offers more possibilities for droplet maneuverability over complex terrain. In particular, benefiting from the robust control by the DUT, a droplet can be rationally manipulated against gravity. As shown in Fig. 2D and movie S10, a 4-μl droplet can generate a reciprocating motion in the vertical direction to endow an antigravity droplet transport without any further assistance, which is the maximum droplet volume that the existing DUT can precisely manipulate.

To summarize, the DUT not only enables contactless, rapid, and precise droplet manipulation in programmable paths on a horizontal superhydrophobic surface but can also achieve several dexterous capabilities including traversing narrow slits, crossing steep slopes,

and moving against gravity in a reciprocating motion. The DUT demonstrates the universal adaptability to surfaces and droplets, eliminating their need for the pretreatment. As depicted in Fig. 2E, this manipulation technique is superior or even unparalleled in eight aspects compared with previously reported representative studies using other external fields. "Y", "N," and "NG" in the graph indicate yes, no, and not given in the literature, respectively.

Manipulation mechanism of the DUT

To reveal the underlying mechanism of droplet manipulation of DUT, we analyze the forces acting on the droplet in the twin trap ultrasonic field. Two kinds of forces exert on the drop that could be responsible for its propulsive movement on a horizontal superhydrophobic surface, including the acoustic radiation force F_A and the lateral adhesion force F_{ad}. Then, the net force F driving the droplet could be expressed as $F = F_A - F_{ad}$, which provides a fundamental understanding of droplet motion in the twin trap. Note that the force acting against the droplet movement F_{ad} is a constant, which could be expressed as $F_{ad} = kw\gamma_{LV}(\cos\theta_R - \cos\theta_A)$, with k, w, γ_{LV}, θ_R, and θ_A being the shape correction coefficient, the width of the water droplet, the liquid-vapor surface tension, receding contact angle, and advancing contact angle, respectively. Hence, central to this discussion is the acoustic radiation force F_A acting on the droplet as it moves on the surface. Note that F_A is the integral of the acoustic radiation pressure P_A over the entire surface of the droplet (*33*) as

$$F_A = -\int_{S_0} P_A \mathbf{n} dS \quad (1)$$

where $\mathbf{n}$ is the normal unit vector pointing outward from the surface S_0 and P_A is calculated according to King's theory (*34*) as

$$P_A = \frac{1}{2\rho_0 c_0^2}\langle p^2\rangle - \frac{1}{2}\rho_0\langle v^2\rangle \quad (2)$$

where p is the acoustic pressure amplitude, ρ_0 is the density of air, c_0 is the sound speed in air, and v is the medium particle velocity of air. The angular brackets in Eq. 2 denote the time average over one cycle of acoustic oscillation. The first term represents the high acoustic pressure region exerting a positive pressure over the droplet surface, while the second term implies the Bernoulli effect representing the oscillation of the air particles exerting a negative pressure on the droplet (*35*). However, it is extremely difficult to determine F_A exerted on the droplet because of the sensitivity of the twin trap ultrasonic field.

To address this challenge, the distribution of acoustic pressure amplitude p and velocity amplitude v was determined by performing an acoustic simulation using the commercial finite element software COMSOL Multiphysics 5.6. The configuration of the simulation domain is consistent with the geometry of the DUT, and the droplet was set in an ellipsoidal shape to resemble its actual shape geometry in Fig. 1F. More details about the numerical model are given in note S1. Figure 3 (A to C) shows the cross section of a 2-μl droplet cutting through its center on three typical positions in the twin trap. The color shadings represent the acoustic pressure amplitude p, velocity amplitude v, and the acoustic radiation pressure P_A, respectively. The red arrows represent the relative magnitude and direction of the acoustic radiation force F_A. Position 1 is exactly at the center of the twin trap, i.e., the focal point, where a droplet is subjected to a holosymmetric F_A resulting from the combination of axisymmetric acoustic pressure amplitude p and velocity amplitude v (Fig. 3A), enabling a stable droplet trapping. Note that this special distribution of the acoustic radiation force over the droplet surface endows a deformed droplet shape by the compression in the x direction and the stretching in the y direction, i.e., an ellipsoid as shown in Fig. 1F (*36*, *37*). Position 2 is on the x axis at $x = -1.5$ mm from the focal point, where a nonaxisymmetry acoustic pressure amplitude mainly contributed to the imbalanced acoustic radiation force in the x direction (Fig. 3B), enabling the droplet to move toward the focal point. Similarly, position 3 is on the y axis at $y = -1$ mm from the focal point, where a nonaxisymmetry velocity amplitude lead to the imbalanced acoustic radiation force in the y direction (Fig. 3C), forcing the droplet to head toward the focal point as well. Such a result well explained why the droplet can be trapped at the focal point by the twin trap. However, specific magnitude of F_A obtained from this simulation is inaccurate, owing to the gas-liquid interface being set to a fully reflective boundary condition.

To further figure out the strength of the acoustic radiation force F_A, the acceleration of the droplet is determined experimentally by recording its dynamic behavior. Figure 3 (D and E) shows the calculated acceleration (a) and displacement (s) of a 2-μl droplet when the focal point is changed for 1 mm along the x and y axes, respectively, illustrating that the wavy force profile experienced by the moving droplet enables its damping oscillation. Note that the maximum acceleration (a_{max}) along x axis is much higher than that along y axis, making the droplet a smaller amplitude of oscillation and stabilize more quickly in the former case. On the basis of Newton's second law, the maximum acoustic radiation force F_M during droplet motion is calculated to be ~80 μN, which is large enough to overcome the lateral adhesive forces from the surface (~1 μN) and its gravity (~20 μN). Therefore, compared with other techniques, our strategy endows an enhanced performance (Fig. 3F), and thus enables a versatile droplet manipulation outlined above.

Multifunctional applications of the DUT

The robust and versatile droplet manipulation of DUT can be harnessed in some unique scenarios including ballistic ejection and droplet dispensing. Figure 4A presents selected snapshots of the loading and ejecting process of a 6-μl droplet in a triangular slit using DUT. As the droplet squeezes into the slit, it undergoes an increasing deformation characterized by further elongation within the diverging side walls. Once the DUT is switched off, the elongated droplet is ejected instantly with a velocity of up to 100 mm/s, reminiscent of the release of a slingshot (movie S11). Such a high-speed droplet ejection provides an effective means for directional fixed-velocity droplet launching and rheological measurement (*38*), which has never been reported before. Figure 4B further illustrates the capability of the DUT to perform droplet dispensing. When a 5-μl droplet is navigated over an array of circular hydrophilic patches with a diameter of 1 mm, each hydrophilic patch retains a small portion of liquid within the boundary of the hydrophilic patch, leaving behind an array of daughter droplets correspondingly, while the majority of the droplet travels ahead along the trajectory of the focal point (movie S12), which is valuable for contactless microdroplet distribution in biochemical detection (*39*). In addition, droplets can be maneuvered to carry out chemical reactions,

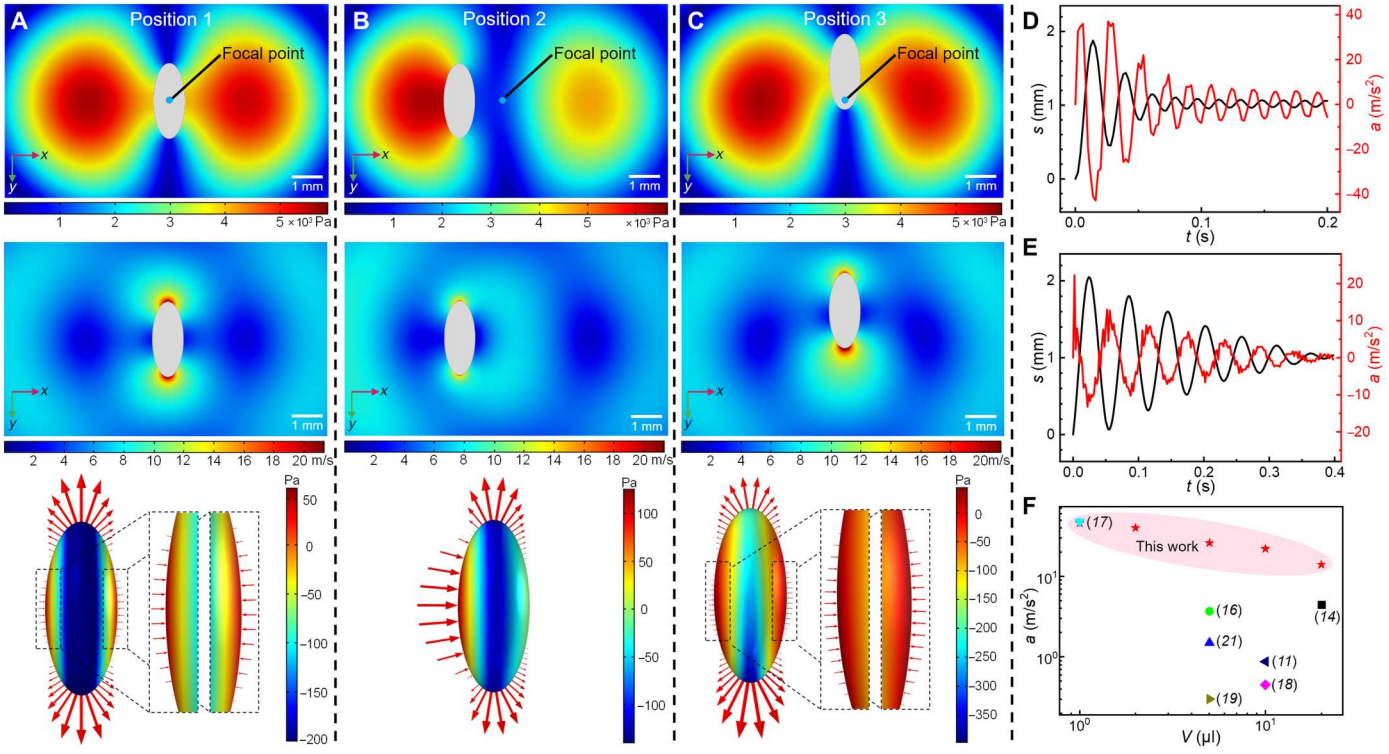

Fig. 3. Manipulation mechanism of the droplet ultrasonic tweezer (DUT). (**A** to **C**) Three typical positions of the droplet in the twin trap ultrasonic field. The three rows represent the distribution of acoustic pressure amplitude *p*, the distribution of velocity amplitude *v*, and the distribution of the acoustic radiation pressure P_A, respectively. The acoustic radiation force F_A is indicated in the third row with red arrows. (**D**) Calculated acceleration (*a*) and displacement (*s*) of a 2-μl droplet when the focal point is changed for 1 mm along the *x* axis. (**E**) Calculated acceleration (*a*) and displacement (*s*) of a 2-μl droplet when the focal point is changed for 1 mm along the *y* axis. (**F**) Acceleration suffered by the droplet in DUT compared with other techniques.

such as color reaction. As shown in Fig. 4C, a 4-μl acetic acid aqueous droplet is guided by the DUT to merge with a 4-μl litmus droplet, resulting in a color change from purple to orange after reaction. The merged droplet can break free from the anchoring hydrophilic point and be guided to the specified destination (movie S13). The sequential images in Fig. 4D further demonstrate the cleaning function of the DUT, e.g., a 10-μl droplet could clean the stains precisely in real time (movie S14).

DISCUSSION

In summary, a DUT based on phased array has been demonstrated for multifunctional droplet manipulation on superhydrophobic surfaces. A twin trap ultrasonic field was generated by the DUT, which can trap the droplet at the position of the focal point. The droplet can move along arbitrary paths and stop precisely within a wide volume range, i.e., 0.5 to 65 μl, and a high maximum speed, e.g., 250 mm/s, by moving the focal point step by step programmatically. Benefiting from the broad and robust effect of the twin trap, the DUT grants the droplet the unprecedented ability to pass through slits narrower than its own diameter up to 2.5 times without any further assistance and enables the droplet to cross steep slopes with a maximum inclination of 80° or higher than its own diameter. Furthermore, the droplet can move against gravity in a reciprocating motion under the powerful control of the DUT. Numerical simulation reveals that the droplet is subjected to an asymmetric acoustic radiation force, making it move toward the focal point and stabilize quickly. Our work further demonstrates that the DUT can be cleverly harnessed for droplet ejection, droplet dispensing, chemical reactor, and surface cleaning, which would open promising avenues for multifunctional droplet manipulation without surface and droplet pretreatment.

MATERIALS AND METHODS

Experimental setup

The control system of the DUT consists of a laptop, a driver board, and 28 ultrasound transducers (MSO-P2Z1040AH07T, Manorshi, China), as shown in fig. S5A. Twenty-eight transducers are chosen for lower energy consumption and reliable droplet control. The transducers on the upper layer are inclined downward by 30° to maximize the ultrasonic intensity. The control software is used to calculate the acoustic pressure amplitude distribution on a specific focal point and send the phase delays to the driver board, which generates square wave signals with different phases (18 Vpp and 40 kHz with a resolution of π/5°) and sends them to the transducers. The bracket array with the material of acrylic photosensitive resin (Rayshape Intelligence Technology Co. Ltd) was fabricated by a three-dimensional (3D) printer (Shape1 HD, Rayshape, China).

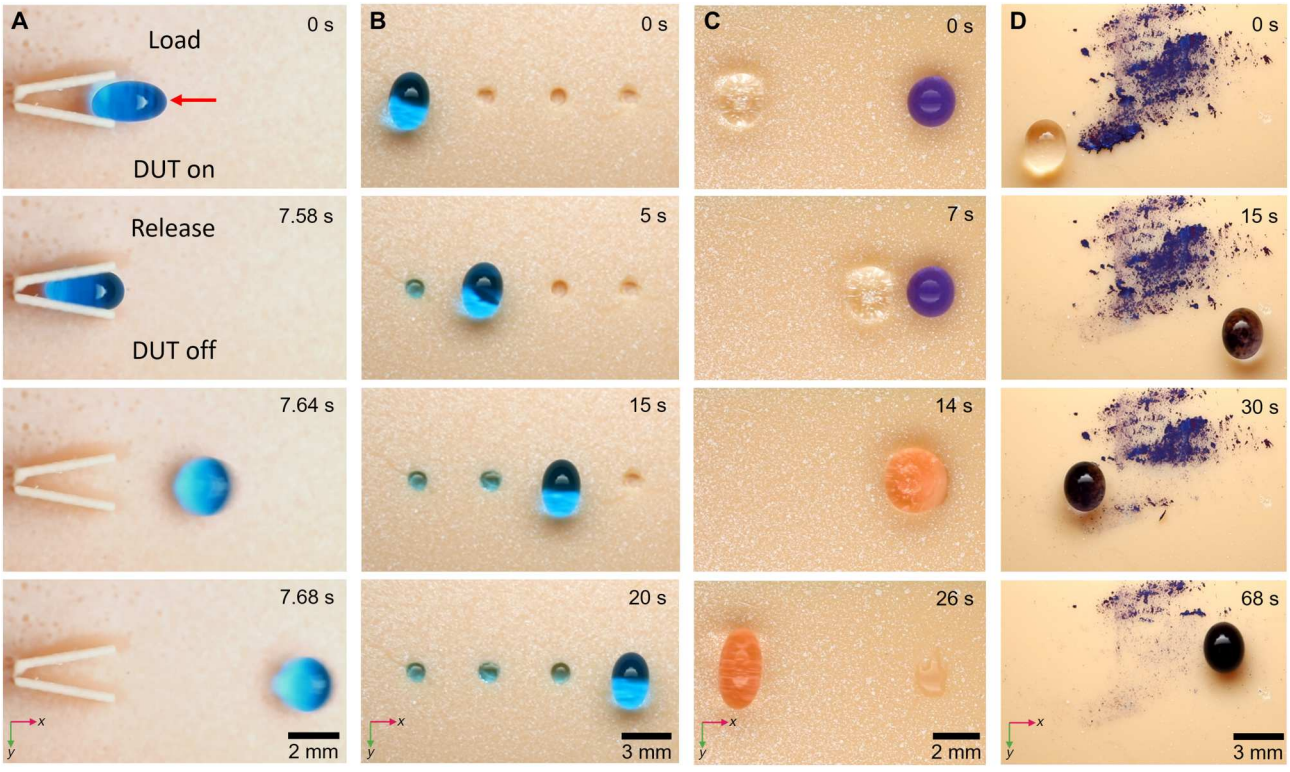

Fig. 4. The applications of the droplet ultrasonic tweezer (DUT). (**A**) A 6-μl droplet ballistic ejection at $A = 0.5$. (**B**) A 5-μl droplet dispensing at $A = 1$. (**C**) A 4-μl acetic acid aqueous droplet is guided by the DUT at $A = 0.3$ to react with a 4-μl litmus droplet and then guided back at $A = 0.4$ after reaction. (**D**) Surface-cleaning application of the DUT using a 10-μl droplet at $A = 0.2$.

Fabrication of superhydrophobic surfaces

The superhydrophobic surfaces were prepared from 1060 aluminum plates. Specifically, the plate with a thickness of 2 mm was polished by nos. 500 and 1200 abrasive papers in sequence, followed by ultrasonically cleaning in ethanol and deionized water for 10 min, respectively. After immersing in boiling water for ~40 min, the surface was uniformly coated with cross-linked nanosheets, followed by silanization by immersion in 1 mM *n*-hexane solution of trichloro-(1*H*, 1*H*, 2*H*, 2*H*)-perfluorooctylsilane for ~1 hour and heat treatment at 150°C in air for 1 hour to render the whole surface superhydrophobic with an apparent contact angle over 159°, as shown in fig. S5B. The topographical surfaces used in the experiment were prepared by a 3D printer described above. A commercially available coating (XN-204B, Xinnano, China) was sprayed uniformly onto the surface to render it superhydrophobic.

Characterization

The surface structure was characterized by a scanning electron microscope (SU5000, Japan). The static contact angle on the surface was measured from sessile water drops with an OCA25 system (DataPhysics Instruments GmbH, Germany) for a droplet of ~4 μl. At least five individual measurements were conducted on the surface. During the experiment, deionized water droplets were first placed on the superhydrophobic surface by a micropipette, and the dynamic behavior was filmed from the top or side view using a single-lens reflex camera (EOS 5D MarkIV, Cannon, Japan). The data in Fig. 3 (D to F) and fig. S2 (B and C) were obtained by analyzing videos recorded by a high-speed camera (FASTCAM SA5, Photron Limited) at a frame rate of 500 fps, and the droplet motion in movies S4 and S8 were recorded by the high-speed camera at a frame rate of 10,000 fps.

Supplementary Materials

This PDF file includes:
Note S1
Figs. S1 to S6
Legends for movies S1 to S14

Other Supplementary Material for this manuscript includes the following:
Movies S1 to S14

REFERENCES AND NOTES

1. I. Hajji, M. Serra, L. Geremie, I. Ferrante, R. Renault, J.-L. Viovy, S. Descroix, D. Ferraro, Droplet microfluidic platform for fast and continuous-flow RT-qPCR analysis devoted to cancer diagnosis application. *Sens. Actuators B Chem.* **303**, 127171 (2020).
2. L. Zhang, J. Sun, H. He, Y. Huang, H. Shi, W. Chen, Microdroplet extraction assisted ultrasensitive Raman detection in complex oil. *Lab Chip* **21**, 2217–2222 (2021).
3. A. C. Sun, D. J. Steyer, A. R. Allen, E. M. Payne, R. T. Kennedy, C. R. J. Stephenson, A droplet microfluidic platform for high-throughput photochemical reaction discovery. *Nat. Commun.* **11**, 6202 (2020).
4. J. Wang, P. H. Chao, S. Hanet, R. M. van Dam, Performing multi-step chemical reactions in microliter-sized droplets by leveraging a simple passive transport mechanism. *Lab Chip* **17**, 4342–4355 (2017).
5. Z. Yu, T. Zhu, J. Zhang, M. Ge, S. Fu, Y. Lai, Fog harvesting devices inspired from single to multiple creatures: Current progress and future perspective. *Adv. Funct. Mater.* **32**, 2200359 (2022).

6. Y. Zheng, H. Bai, Z. Huang, X. Tian, F.-Q. Nie, Y. Zhao, J. Zhai, L. Jiang, Directional water collection on wetted spider silk. *Nature* **463**, 640–643 (2010).
7. P. Zhu, R. Chen, C. Zhou, Y. Tian, L. Wang, Asymmetric fibers for efficient fog harvesting. *Chem. Eng. J.* **415**, 128944 (2021).
8. C. Liu, C. Lu, Z. Yuan, C. Lv, Y. Liu, Steerable drops on heated concentric microgroove arrays. *Nat. Commun.* **13**, 3141 (2022).
9. J. Li, Y. Hou, Y. Liu, C. Hao, M. F. Li, M. K. Chaudhury, S. Yao, Z. Wang, Directional transport of high-temperature Janus droplets mediated by structural topography. *Nat. Phys.* **12**, 606–612 (2016).
10. X. Liang, V. Kumar, F. Ahmadi, Y. Zhu, Manipulation of droplets and bubbles for thermal applications. *Droplet* **1**, 80–91 (2022).
11. G. Chen, Z. Dai, S. Li, Y. Huang, Y. Xu, J. She, B. Zhou, Magnetically responsive film decorated with microcilia for robust and controllable manipulation of droplets. *ACS Appl. Mater. Interfaces* **13**, 1754–1765 (2021).
12. S. Ben, T. Zhou, H. Ma, J. Yao, Y. Ning, D. Tian, K. Liu, L. Jiang, Multifunctional magneto-controllable superwettable-microcilia surface for directional droplet manipulation. *Adv. Sci. (Weinh)* **6**, 1900834 (2019).
13. C. Yang, Z. W. Zhang, G. Li, Programmable droplet manipulation by combining a superhydrophobic magnetic film and an electromagnetic pillar array. *Sens. Actuators B Chem.* **262**, 892–901 (2018).
14. Y. Zhang, S. Jiang, Y. Hu, T. Wu, Y. Zhang, H. Li, A. Li, Y. Zhang, H. Wu, Y. Ding, E. Li, J. Li, D. Wu, Y. Song, J. Chu, Reconfigurable magnetic liquid metal robot for high-performance droplet manipulation. *Nano Lett.* **22**, 2923–2933 (2022).
15. A. Li, H. Li, Z. Li, Z. Zhao, K. Li, M. Li, Y. Song, Programmable droplet manipulation by a magnetic-actuated robot. *Sci. Adv.* **6**, eaay5808 (2020).
16. Y. Jin, W. Xu, H. Zhang, R. Li, J. Sun, S. Yang, M. Liu, H. Mao, Z. Wang, Electrostatic tweezer for droplet manipulation. *Proc. Natl. Acad. Sci. U.S.A.* **119**, e2105459119 (2022).
17. Q. Sun, D. Wang, Y. Li, J. Zhang, S. Ye, J. Cui, L. Chen, Z. Wang, H.-J. Butt, D. Vollmer, X. Deng, Surface charge printing for programmed droplet transport. *Nat. Mater.* **18**, 936–941 (2019).
18. J. Nie, Z. Ren, J. Shao, C. Deng, L. Xu, X. Chen, M. Li, Z. L. Wang, Self-powered microfluidic transport system based on triboelectric nanogenerator and electrowetting technique. *ACS Nano* **12**, 1491–1499 (2018).
19. H. Dai, C. Gao, J. Sun, C. Li, N. Li, L. Wu, Z. Dong, L. Jiang, Controllable high-speed electrostatic manipulation of water droplets on a superhydrophobic surface. *Adv. Mater.* **31**, e1905449 (2019).
20. W. Yan, C. Zhao, W. Luo, W. Zhang, X. Li, D. Liu, Optically guided pyroelectric manipulation of water droplet on a superhydrophobic surface. *ACS Appl. Mater. Interfaces* **13**, 23181–23190 (2021).
21. W. Li, X. Tang, L. Wang, Photopyroelectric microfluidics. *Sci. Adv.* **6**, eabc1693 (2020).
22. X. Tang, L. Wang, Loss-free photo-manipulation of droplets by pyroelectro-trapping on superhydrophobic surfaces. *ACS Nano* **12**, 8994–9004 (2018).
23. M. A. Ghanem, A. D. Maxwell, Y.-N. Wang, B. W. Cunitz, V. A. Khokhlova, O. A. Sapozhnikov, M. R. Bailey, Noninvasive acoustic manipulation of objects in a living body. *Proc. Natl. Acad. Sci. U.S.A.* **117**, 16848–16855 (2020).
24. R. Hirayama, D. Martinez Plasencia, N. Masuda, S. Subramanian, A volumetric display for visual, tactile and audio presentation using acoustic trapping. *Nature* **575**, 320–323 (2019).
25. D. Zang, Y. Yu, Z. Chen, X. Li, H. Wu, X. Geng, Acoustic levitation of liquid drops: Dynamics, manipulation and phase transitions. *Adv. Colloid Interface Sci.* **243**, 77–85 (2017).
26. D. Foresti, M. Nabavi, M. Klingauf, A. Ferrari, D. Poulikakos, Acoustophoretic contactless transport and handling of matter in air. *Proc. Natl. Acad. Sci. U.S.A.* **110**, 12549–12554 (2013).
27. H. Bruus, Acoustofluidics 7: The acoustic radiation force on small particles. *Lab Chip* **12**, 1014–1021 (2012).
28. A. Watanabe, K. Hasegawa, Y. Abe, Contactless fluid manipulation in air: Droplet coalescence and active mixing by acoustic levitation. *Sci. Rep.* **8**, 10221 (2018).
29. M. A. B. Andrade, T. S. A. Camargo, A. Marzo, Automatic contactless injection, transportation, merging, and ejection of droplets with a multifocal point acoustic levitator. *Rev. Sci. Instrum.* **89**, 125105 (2018).
30. A. Marzo, S. A. Seah, B. W. Drinkwater, D. R. Sahoo, B. Long, S. Subramanian, Holographic acoustic elements for manipulation of levitated objects. *Nat. Commun.* **6**, 8661 (2015).
31. A. Marzo, B. W. Drinkwater, Holographic acoustic tweezers. *Proc. Natl. Acad. Sci. U.S.A.* **116**, 84–89 (2018).
32. A. Marzo, T. Corkett, B. W. Drinkwater, Ultraino: An open phased-array system for narrowband airborne ultrasound transmission. *IEEE Trans. Ultrason. Ferroelectr. Freq. Control* **65**, 102–111 (2018).
33. W. Di, Z. Zhang, L. Li, K. Lin, J. Li, X. Li, B. P. Binks, X. Chen, D. Zang, Shape evolution and bubble formation of acoustically levitated drops. *Phys. Rev. Fluids* **3**, 103606 (2018).
34. L. V. King, On the acoustic radiation pressure on spheres. *Proc. R. Soc. Lond. Ser. A* **147**, 212–240 (1934).
35. M. A. B. Andrade, A. Marzo, Numerical and experimental investigation of the stability of a drop in a single-axis acoustic levitator. *Phys. Fluids* **31**, 117101 (2019).
36. Q. Shi, W. Di, D. Dong, L. W. Yap, L. Li, D. Zang, W. Cheng, A general approach to free-standing nanoassemblies via acoustic levitation self-assembly. *ACS Nano* **13**, 5243–5250 (2019).
37. D. Zang, J. Li, Z. Chen, Z. Zhai, X. Geng, B. P. Binks, Switchable opening and closing of a liquid marble via ultrasonic levitation. *Langmuir* **31**, 11502–11507 (2015).
38. Y. Tian, R. G. Holt, R. E. Apfel, Investigation of liquid surface rheology of surfactant solutions by droplet shape oscillations: Experiments. *J. Colloid Interface Sci.* **187**, 1–10 (1997).
39. H. Cui, T. Tronser, X. Wang, J. Wesslowski, G. Davidson, A. A. Popova, P. A. Levkin, High-throughput formation of miniaturized cocultures of 2D cell monolayers and 3D cell spheroids using droplet microarray. *Droplet* **2**, e39 (2023).

Acknowledgments

Funding: This work was supported by the National Key Research and Development Program of China (2022YFB4602401), the National Natural Science Foundation of China (52075071), Opening Project of the Key Laboratory of Bionic Engineering (Ministry of Education), the Jilin University (KF20200002), and the Key Laboratory of Icing and Anti/De-icing of CARDC (IADL 20210405). **Author contributions:** Z.Y. and Y.L. conceived the project. Y.L. supervised the project. Z.Y., C. Lu, and C. Liu designed the project. Z.Y., C. Lu, and X.B. performed the experiments. Z.Y., S.F., and L.Z. analyzed the data. All the authors contributed to manuscript writing and editing. **Competing interests:** The authors declare that they have no competing interests. **Data and materials availability:** All data needed to evaluate the conclusions in the paper are present in the paper and/or the Supplementary Materials.

Submitted 11 December 2022
Accepted 16 March 2023
Published 19 April 2023
10.1126/sciadv.adg2352